

Test of internal-conversion theory with measurements in ^{134}Cs and ^{137}Ba

N. Nica,^{*} J. C. Hardy, V. E. Jacob, and W. E. Rockwell[†]
Cyclotron Institute, Texas A&M University, College Station, Texas 77843, USA

M. B. Trzhaskovskaya
Petersburg Nuclear Physics Institute, Gatchina RU-188300, Russia

(Received 14 November 2006; published 23 February 2007)

We have measured the ratio of K -shell internal conversion coefficients, α_K , for the 127.5-keV $E3$ transition in ^{134}Cs and the 661.7-keV $M4$ transition in ^{137}Ba . Previous measurements of these α_K values led to a ratio that differed from calculated internal conversion coefficients. Our measured result, 30.01(15), disagrees with, but is a factor of three more precise than, the previous average of all experimental results. Our new result is consistent with calculations.

DOI: [10.1103/PhysRevC.75.024308](https://doi.org/10.1103/PhysRevC.75.024308)

PACS number(s): 23.20.Nx, 27.60.+j

I. INTRODUCTION

Internal conversion is a ubiquitous feature of decay schemes for all but the lightest nuclei. Calculations of tabulated internal conversion coefficients (ICCs) have appeared over the years [1–5] and, in their turn, have been routinely employed in the derivation of decay schemes based on experimental measurements of γ rays. As computational techniques improved over time, the calculated ICC values changed somewhat and naturally it was always presumed that their reliability was improving even though, until recently, relatively few precise measurements of the conversion coefficients themselves had actually been made. In fact, the few that did exist were not in particularly good agreement with the tabulated values, leading Raman *et al.* [6] to conclude in 1973 that there was a systematic discrepancy at that time between experiment and theory of 2–3% for $E3$ and $M4$ transitions. For nearly the next three decades there was little reason to change this conclusion.

The situation improved considerably in 2002 with the publication of new ICC tables by Band *et al.* [5] calculated in the framework of the Dirac-Fock method and, for the first time, with the exchange between electrons treated exactly. A new survey of ICC data [7] published in the same year compared this new tabulation—as well as some earlier ones—to world data and found that the Band *et al.* tables agreed to within a few tenths of a percent on average. This was nearly an order-of-magnitude improvement over the earlier ICC tabulations. One problem remained however: the data appeared to show a preference for one particular model—the one actually used by Band *et al.*—in which the final-state electron wave function was computed in a field that did not include the atomic subshell vacancy caused by the conversion process. In effect this calculation assumed that the vacancy is filled before the conversion electron leaves the atom, even

though a simple comparison of the known vacancy lifetimes with transit times for escaping electrons shows that this cannot be so [8].

This curious contradiction was settled several years later by our precise measurement of the K -shell conversion coefficient, α_K , for the 80.2-keV $M4$ transition in ^{193}Ir [9,10]. This α_K value if calculated without the vacancy is 10% smaller than if the vacancy is included, a difference that is the largest calculated for any accessible transition. The experimental result, which was obtained with 0.8% precision, agreed precisely with the ICC value calculated including the vacancy. Unfortunately, though, while our result clearly confirmed the physically reasonable presence of the vacancy, other ICCs calculated under the same prescription did not agree quite as well with the previously existing body of world data (see Figs. 7 and 8 in Ref. [7]). They deviated on average by about 1%. This was certainly better agreement than had been possible with the older calculations but it was significantly worse than that obtained with the same Dirac-Fock calculations with the vacancy ignored (as published in Ref. [5]).

However, since very few high-precision ($\leq 1\%$) ICC measurements exist, it is not clear how seriously one should view a 1% discrepancy between experiment and theory, which is only discernible in the average over many different transitions—not to mention that the measurements themselves were published over a span of more than five decades and may not all be equally reliable. Of more concern, in our view, are several cases in which ICCs determined with reasonable precision differ by more than two standard deviations from both versions of the modern Dirac-Fock calculations: i.e., whether the atomic vacancy is included or not. There are three such cases known [7,8]: two $E3$ transitions, a 128-keV one in ^{134}Cs and a 40-keV one in ^{103}Rh , and a 347-keV $M4$ transition in ^{197}Pt . If taken at face value, these three discrepant cases could indicate that there is some further aspect of the theory that is not quite complete. In this paper, we address one of these cases: the K -shell conversion of the $E3$ transition in ^{134}Cs , a transition which is cleanly observed in the decay of a 2.9-h isomeric state at 139 keV.

^{*}Electronic address: nica@comp.tamu.edu

[†]REU summer student from Mount Holyoke College, South Hadley, MA 01075.

II. MEASUREMENT OVERVIEW

The K -shell internal conversion coefficient, α_K , for a particular transition is defined to be the ratio of the probability for internal conversion onto a K -shell electron relative to the probability for emitting a γ -ray: viz. $\alpha_K = \lambda_{eK}/\lambda_\gamma$. Each electron vacancy created in the K shell produces K x rays with a probability equal to the K -shell fluorescence yield, ω_K . Thus, if only a single transition is involved and a spectrum of x rays and γ rays is recorded for its decay, the ratio of the total number of K x rays observed, N_K , to the total number of γ rays, N_γ , relates to the K -shell ICC by the simple relationship

$$\alpha_K \omega_K = \frac{N_K}{N_\gamma} \cdot \frac{\epsilon_\gamma}{\epsilon_K}, \tag{1}$$

where ϵ_K and ϵ_γ are the detector efficiencies for the x rays and γ rays, respectively. Fluorescence yields have been well measured for cesium and the nearby elements [11]. They have also recently been evaluated as a function of Z [12] for all elements with $10 \leq Z \leq 100$, and ω_K values have been recommended, which have an uncertainty of about 0.5% around $Z = 55$. Thus, Eq. (1) allows α_K to be extracted directly from measured peak areas with subpercent precision provided that the detector efficiencies are sufficiently well known.

The decay scheme of the 2.9-h isomer in ^{134}Cs is shown in Fig. 1. The predominant decay path is via the cascaded transitions with energies of 127.5 keV and 11.2 keV, the former being the $E3$ transition of interest here. All three transitions shown in the figure convert, but the 11.2-keV transition can only convert in the L and higher shells, and the direct 138.7-keV transition to the ground state is nearly a factor of 200 weaker than the 127.5-keV transition. Thus, the K -x-ray peak observed in a decay spectrum of $^{134}\text{Cs}^m$ can easily be corrected for the small contribution from the 138.7-keV transition, leaving the remainder as being due entirely to conversion of the 127.5-keV transition. This satisfies the ‘‘single transition’’ requirement for the validity of Eq. (1).

One serious difficulty remains, however. Our ORTEC Gamma-X HPGe detector—a 280-cm³ n-type coaxial

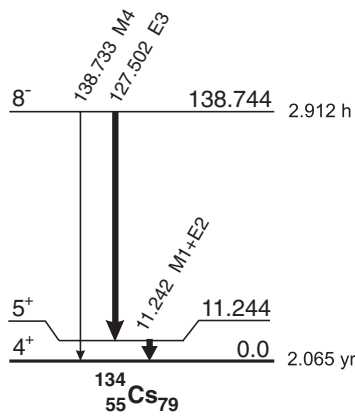


FIG. 1. Decay scheme for the decay of the 2.9-h isomeric state in ^{134}Cs . The information is taken from Ref. [13]. Note that the strong transitions are shown with heavy arrows. The weak 139-keV transition accounts for $\sim 0.5\%$ of decay from the isomer (including the effects of internal conversion).

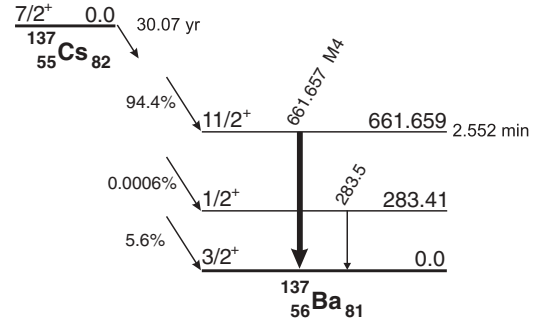


FIG. 2. Decay scheme for the β decay of ^{137}Cs . The information is taken from Ref. [13]. The strong transition is shown with a heavy arrow.

crystal—has been meticulously calibrated [14,15] to a relative precision of 0.15% (and 0.20% absolute), but this precision applies only between 50 and 1400 keV. The K x rays of cesium lie between 30 and 36 keV, well below this region. Although we have in fact calibrated our detector to lower energies (and to higher [16]), our standards in the lower-energy region depend themselves on calculated conversion coefficients. We can hardly use a calibration standard based on previously calculated ICCs to test the validity of a newly calculated ICC.

Our solution to this problem was to measure the α_K of a second transition with a similar x-ray energy in addition to the one in ^{134}Cs and to compare the ratio of the two ICCs with theory. Our additional measurement was of the spectrum of x and γ rays observed following the β decay of ^{137}Cs . The relevant decay scheme appears in Fig. 2. Once again, only a single transition is effectively involved and Eq. (1) can be applied to the measured spectrum. If we denote the result from ^{134}Cs with the subscript 1 and that from ^{137}Cs decay by 2, then the ratio of the two K -conversion coefficients is given by

$$\frac{\alpha_{K1}}{\alpha_{K2}} = \frac{\omega_{K2}}{\omega_{K1}} \cdot \frac{N_{K1}N_{\gamma 2}}{N_{\gamma 1}N_{K2}} \cdot \frac{\epsilon_{\gamma 1}}{\epsilon_{\gamma 2}} \cdot \frac{\epsilon_{K2}}{\epsilon_{K1}}. \tag{2}$$

Here the efficiencies in the K x-ray region, ϵ_{K1} and ϵ_{K2} , appear only in a ratio. The crucial feature of the two decays we have chosen is that the x rays of cesium (from $^{134}\text{Cs}^m$ decay) lie only about 1.3 keV below those of barium (from ^{137}Cs decay) and, in this energy region (around 33 keV), the efficiency of our detector changes by only 0.38%/keV, a small amount whose uncertainty is completely negligible in the present context. Thus, by evaluating the ratio of α_K values for the 127.5-keV transition in ^{134}Cs and the 661.7-keV transition in ^{137}Ba , we eliminate the need to know the detector efficiency at ~ 33 keV. Instead, the ratio of efficiencies, $\epsilon_{K2}/\epsilon_{K1} = 1.0048(3)$, simply becomes a small and reliable correction term in the analysis of our measurements.

In measuring the ratio of conversion coefficients we also preserve the original purpose of our study: to test the recent Dirac-Fock ICC calculations. These calculations produce values for the ratio $\alpha_K(^{134}\text{Cs})/\alpha_K(^{137}\text{Ba})$ of 29.5 if the K -shell vacancy is ignored and 30.0 if it is included in the ‘‘frozen orbital’’ approximation [7,9]. The previous experimental value obtained from world data [7] was 28.8(5), which conflicts with

both calculations but most significantly from the now-favored version that includes the vacancy. We seek to improve the experimental value to determine if this discrepancy is real.

III. EXPERIMENT

We used the same experimental method and setup as in our previous measurements [9,10]. Only those details not covered in previous publications will be described here.

A. Source preparation

Two sources were required for these measurements: 30.1-yr ^{137}Cs and 2.9-h $^{134}\text{Cs}^m$. Being long-lived and readily available, the former could be purchased; the latter had to be made locally so it could be transported rapidly to our detection equipment. Our ^{137}Cs source was a 37-kBq “conversion electron source” (ME Series) purchased from Isotope Products Laboratories. The manufacturer prepared it by evaporating a 5-mm-diameter spot of the radionuclide on a 6- μm -thick Mylar substrate and protecting it with a 100–200 $\mu\text{g}/\text{cm}^2$ acrylic cover. Although the source thickness is not given by the manufacturer, 37 kBq of activity corresponds to 0.12 μg of ^{137}Cs , which if spread over a 5-mm spot would give negligible self-absorption. No noticeable attenuation would be expected from the thin acrylic cover either.

Because of its 2.9-h half-life, we had to produce $^{134}\text{Cs}^m$ sources ourselves by neutron activation of natural cesium, which is monoisotopic (^{133}Cs). For the same reason, we also found it necessary to prepare a uniform layer of material, suitable for a thin source, and irradiate it in that form, rather than irradiating the material first and preparing a source later. As a result, we had to be very careful not to include isotopes in our source material or substrate that could produce interfering activity after activation.

We tested three pure chemicals as candidates for our neutron-activation sample: CsCl (99.999%+), CsNO_3 (99.999%), and Cs_2CO_3 (99.995%). We placed 0.05-ml drops of aqueous solutions of a weighed quantity of each chemical onto a layer of 1/10 diluted wet insulin on a substrate of 76- μm -thick Mylar. Because two of the chemicals are hygroscopic, we dried all samples in vacuum and subsequently stored them in a dry nitrogen atmosphere. Upon examination, the Cs_2CO_3 samples proved to be considerably less homogeneous than the ones made from CsCl and CsNO_3 , so they were not used for activation.

Previous tests had shown us that activated Mylar contains a number of radioactivities, of which Br and Sb are intense enough to be a concern but not enough to compromise a good measurement; activated Kapton, however, contains much larger quantities of Br. We therefore covered our samples initially with a dimpled Mylar cover that was sealed with tape at the edges. A sample to be activated was then placed in a thermal-neutron flux of $\sim 7 \times 10^{12}$ n/cm² s for 30 min at the TRIGA reactor in the Texas A&M Nuclear Science Center. After activation, the Mylar cover was removed from the source and was replaced with an adhesive Kapton layer 64 μm thick. The thin plastic assembly was then trimmed to a disc, 13 mm in diameter, with the contained radioactive spot being 7 mm in diameter.

We prepared two sources in two separate activations several weeks apart: one, designated $T1$, was made from CsCl and the other, designated $T2$, was from CsNO_3 . The derived weights of the samples themselves were 18 and 20 μg , respectively, which corresponds to source thicknesses of 0.10 and 0.14 μm . With these thicknesses, we would expect no self-absorption, although some attenuation of x and γ rays must of course occur in the Kapton covers. This can be calculated and was easily accounted for in the data analysis.

B. Radioactive decay measurements

We acquired spectra from both sources using the same equipment and procedures as we have described in a previous publication [9]. In the case of ^{137}Cs , our long-lived source, a high-statistics spectrum was recorded at low counting rate. For our activated sources of $^{134}\text{Cs}^m$, in all we obtained five spectra from the $T1$ source (labeled $T1.1$ through $T1.5$) and four from $T2$ ($T2.1$ through $T1.4$). All spectra covered the energy interval 10–2000 keV with a dispersion of about 0.25 keV/channel. The first three spectra with source $T1$ and the first two with $T2$ were taken within the first day after irradiation (~ 10 half-lives of $^{134}\text{Cs}^m$). The last two spectra in both cases were taken during the next two days and were intended only to identify or confirm contaminant activities and determine their intensities. In the end, not all nine $^{134}\text{Cs}^m$ spectra were analyzed: the first spectrum, $T1.1$, recorded for source $T1$ was acquired at an uncomfortably high count-rate so we decided not to use it; and by the time the second spectrum, $T2.2$, was obtained from source $T2$, the $^{134}\text{Cs}^m$ activity had decayed sufficiently that it was too contaminated by interfering activities to be useful. All other spectra were analyzed thoroughly, with spectra $T1.2$, $T1.3$, and $T2.1$ being the ones we used to extract x - and γ -ray peak areas for the determination of α_K .

IV. ANALYSIS

In our analysis of the data, we followed the same methodology as we did with previous source measurements [9,10]. We first extracted areas for all the x - and γ -ray peaks of interest. Next, we identified impurities, and made appropriate corrections to account for their effects on the peaks required for the determination of α_K . Finally, we dealt with the various small corrections that had to be applied to these peak areas to account for competing transitions, x -ray scattering and the non-Gaussian shape of the x -ray peaks themselves.

A. Peak areas

The spectra in Fig. 3 show the energy regions of interest for this measurement: those including the K x rays in the decays of both $^{134}\text{Cs}^m$ and ^{137}Cs ; and those including the 127.5- and 661.7-keV γ rays. As before [9,10], we determined all peak areas with GF2, the least-squares peak-fitting program in the RADWARE series [17]. In doing so, we used the same fitting procedures as were used in the original detector-efficiency calibration [14–16].

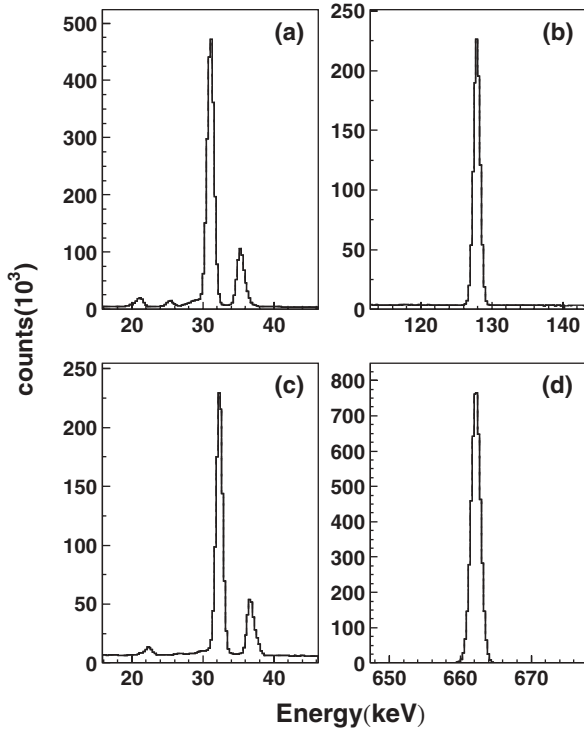


FIG. 3. Spectra for the four energy regions of interest in the determination of the α_K ratio: (a) the cesium x rays from the decay of $^{134}\text{Cs}^m$; (b) the 127.5-keV γ ray from the same decay; (c) the barium x rays from ^{137}Ba , the β -decay daughter of ^{137}Cs ; and (d) the 661.7-keV γ ray also from ^{137}Ba .

Both γ -ray peaks lie on a flat background, well isolated from any other peaks. There is no evidence of competing impurities. The determination of their peak areas presented no difficulties whatsoever.

The x-ray region observed in the spectrum from the decay of ^{137}Cs was also free from contaminant interference (though not from scattering effects), but the same cannot be said of the x-ray region for $^{134}\text{Cs}^m$ decay. Although the impurity contribution to that spectrum is small (see Sec. IV B), it must be carefully accounted for in our analysis. We extracted areas from the x-ray regions of both sources with identical procedures, integrating the total area of the combined K_α and K_β groups between equivalent energy limits. We used a special modification [17] of the GF2 program that allows us to set a background by the normal fitting procedures and then to integrate the total number of counts above that background within set limits, extrapolating a Gaussian tail to account for counts possibly outside those limits. The areas obtained in this way are given in Table I.

B. Impurity identification

We found no evidence of any impurity activities in our purchased ^{137}Cs source. We did observe a number in our activated $^{134}\text{Cs}^m$ sources, although most of them in fact came from the Mylar substrate. After careful analysis of all retained spectra for contaminant activities, we identified γ rays from ^{24}Na , ^{56}Mn , $^{80}\text{Br}^m$, ^{82}Br , ^{122}Sb , ^{124}Sb , and ^{134}Cs (see Fig. 4). Only the last of these, the ground-state decay of ^{134}Cs , was

TABLE I. Peak areas and impurity corrections for the $(K_\alpha + K_\beta)$ x rays from the $^{134}\text{Cs}^m$ and ^{137}Cs sources are given in the upper section, while the peak areas for the relevant γ rays appear in the middle section. The bottom section gives the N_K/N_γ ratios, with further corrections for the competing transition from $^{134}\text{Cs}^m$ and for attenuation in the sample. The remaining correction, for scattering, is applied in Table II.

	$^{134}\text{Cs}^m$ source			^{137}Cs source
	T1.2	T1.3	T2.1	
<i>K</i> x rays:				
Raw <i>K</i> x-ray areas	2717400(5300)	1712200(4400)	2633700(5100)	1904100(4600)
$^{80}\text{Br}^m$ impurity <i>K</i> x rays (%)	-0.18(2)	-0.28(3)	-0.38(4)	
^{122}Sb impurity <i>K</i> x rays (%)	-0.066(2)	-0.292(8)	-0.056(2)	
^{124}Sb impurity <i>K</i> x rays (%)	-0.0088(4)	-0.0473(9)	-0.0074(3)	
^{134}Cs g.s. decay <i>K</i> x rays (%)	-0.046(1)	-0.239(4)	-0.075(1)	
Impurity-corrected <i>K</i> x-ray areas	2709200(5300)	1697600(4400)	2620100(5200)	1904100(4600)
γ rays:				
127.5 keV (^{134}Cs)	1012400(1400)	634200(1200)	977200(1400)	
661.7 keV (^{137}Ba)				7441900(3600)
Ratios N_K/N_γ :				
Impurity-corrected (N_K/N_γ)	2.676(6)	2.677(9)	2.681(7)	0.2559(6)
Weighted average		2.678(4)		
<i>K</i> x rays from 138.7-keV transition (%)		-0.81(5)		
Attenuation in sample (%)		+0.13(1)		
Corrected ratio (except for scattering)		2.660(4)		0.2559(6)

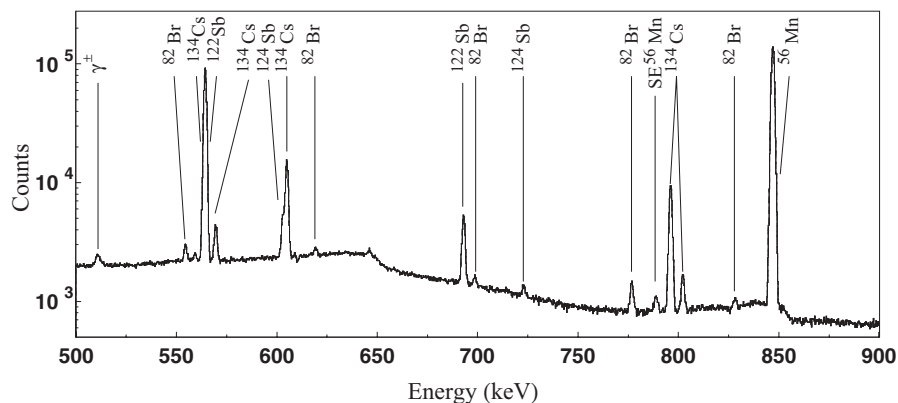


FIG. 4. A portion of the γ -ray energy spectrum $T2.1$, measured soon after the activation of source $T2$. Peaks are identified by their β -decay parent, with “SE” designating a single-escape peak.

produced from the sample material (CsCl or CsNO_3) and it is completely unavoidable. None of these impurities affect the energy region around our γ ray of interest at 127.5 keV but $^{80}\text{Br}^m$, ^{122}Sb , ^{124}Sb , and ^{134}Cs all produce radiation that lies in the same energy region as the cesium x rays. To put this in perspective, though, we note at this point that the total contribution of all these activities to the x-ray peaks of interest turns out to be less than 0.5% of the total in all spectra from which detailed peak areas for $^{134}\text{Cs}^m$ were extracted. At our level of experimental precision, this is not a negligible amount but it is certainly quite manageable. We will briefly deal with each impurity in turn.

$^{80}\text{Br}^m$. In our preliminary studies of the activation of Kapton foil, we observed γ -ray peaks from the decays of both $^{80}\text{Br}^m$ and ^{82}Br , produced from small amounts of bromine contained in the foil material. The strongest peaks by far—and the most numerous—were from ^{82}Br . More difficult to detect was the presence of $^{80}\text{Br}^m$: its decay resulted in only one observable γ -ray peak, at 37.1 keV. The measured half-life of that peak was consistent with the 4.4-h half-life of $^{80}\text{Br}^m$ and no other γ rays with a similar half-life were observed; this is also consistent with $^{80}\text{Br}^m$, whose only other transition, at 48.8 keV, is strongly converted. Unfortunately, the 37.1-keV peak lies just at the edge of the cesium x-ray region and, although it could not be clearly identified in our $^{134}\text{Cs}^m$ -source spectra, the ^{82}Br peaks were certainly observed there (see Fig. 4), indicating that some small amount of $^{80}\text{Br}^m$ must also be present. Because the Kapton-foil measurement had yielded the relative intensities of the $^{80}\text{Br}^m$ and ^{82}Br peaks as a function of time after activation, we could analyze our spectra from sources $T1$ and $T2$ using the relatively strong peaks from ^{82}Br to calculate with good accuracy the intensity of the 37.1-keV γ ray. The result is given in Table I.

^{122}Sb . The decay of 2.7-d ^{122}Sb proceeds both by β^- emission (97.6%) to ^{122}Te and by electron capture (2.4%) to ^{122}Sn , producing x rays characteristic of tellurium and tin. Though these x rays are of lower average energy than those from cesium, the K_β peak from tellurium overlaps with the K_α peak from cesium. We obtained its contribution to the cesium x-ray energy region by two methods: (a) we calculated the x-ray intensity based on the measured intensity of the 564.1-keV γ ray from ^{122}Te and the tabulated properties of

the various decay schemes [13]; and (b) we determined the intensity of the tellurium K_β peak from the measured intensity of the corresponding K_α peak (after we corrected the latter for the contribution of the germanium escape peak from the cesium K_β x ray). Both methods led to similar results, but method (b) was more precise and it is that value which appears in Table I.

^{124}Sb . The evident presence of antimony in our Mylar substrate also led to small amounts of 60.2-d ^{124}Sb , which β^- decays to ^{124}Te . The intensity of the corresponding tellurium x rays was determined from the observed 602.7- and 1691.0-keV γ rays together with the known properties of the decay scheme [13]. The resultant contribution to the cesium x-ray region is negligible, but it is included in Table I for completeness.

^{134}Cs . Neutron capture on cesium produces the 2.07-yr ^{134}Cs ground state an order-of-magnitude more strongly than the 2.9-h isomer we are studying here. Fortunately, the huge half-life differential means that the ground-state decay contributes only weakly to our measured spectra, and the barium x rays it emits play very little role in our analysis. We confirmed this by calculating the x-ray intensity from the observed ^{134}Ba γ rays at 604.7, 795.9 and 802.0 keV; the results are given in Table I.

C. Competing transition

As remarked in Sec. II and illustrated in Fig. 1, in addition to the 127.5-keV transition of interest, the decay of $^{134}\text{Cs}^m$ also includes a weak 138.7-keV transition, whose conversion will also lead to cesium K x rays. Fortunately the latter transition is weak enough that its contribution to the x-ray peak is less than 1% of the total area, and we can account for it to sufficient precision by using the well-measured relative intensity of its γ ray—0.031(4)% [13]—together with α_K values calculated in the Dirac-Fock formalism [5]. (The question of possible few-percent discrepancies in these calculations is irrelevant in this context since the contribution itself is so small.) The resultant correction to the total observed x-ray peak areas appears in Table I with an uncertainty so tiny that it will be seen not to contribute perceptibly to our overall experimental uncertainty.

D. Attenuation in the sample

Although our ^{137}Cs source is thin enough that no attenuation of its x or γ rays should occur, our $^{134}\text{Cs}^m$ source is covered with a Kapton layer, which will have some attenuating effects (see Sec. III A). We calculated the attenuation both of the cesium x rays and of the 127.5-keV γ ray using standard tables of attenuation coefficients [18]. The attenuation is very small, of course, with the x rays suffering 0.13(1)% more than the γ ray. This result is incorporated in Table I.

E. Scattering

In any measurement of this type, some of the photons emitted from the source Compton-scatter from materials in the neighborhood, with the scattered photons then being recorded by the detector. Since the energy of a scattered photon is a function of its scattering angle, each peak of unscattered photons in the detected spectrum exhibits a corresponding continuum of scattered photons that stretches towards lower energies. (This continuum also partly originates from primary or secondary electrons escaping from the sensitive volume of the detector.) How far the continuum stretches depends on the energy of the peak itself. For high-Z x rays and most γ rays, this continuum can usually be ignored since it is spread over an energy range that is much greater than the experimental resolution; consequently it is flat and rather weak in the vicinity of the peak and can easily be accounted for as part of the overall “background” of the peak.

However, for the 30- to 37-keV K x rays from cesium and barium, the scattering continua extend only 3 to 4 keV below the photopeaks and, at our ~ 1 keV resolution, they are only partially distinguishable from those peaks. Although the source-detector environment was identical in our measurements for both sources, the sources themselves differed in the extra thickness of the Mylar substrate for the $^{134}\text{Cs}^m$ source and in the presence of the Kapton cover, both of which would enhance scattering from that source. Matters were further complicated by the weak tin and tellurium x rays observed with the $^{134}\text{Cs}^m$ source (from ^{122}Sb decay—see Sec. IV B), which overlapped the scattering continuum from the cesium x rays. Since the accurate determination of the x-ray peak ratio, N_{K1}/N_{K2} , clearly relies on the proper removal of scattered photons, to establish the size and shape of the continuum is an important goal for us.

We carefully studied this question using the ^{137}Cs source, which was conveniently long lived and was also free of any contaminants in the region below the x-ray peaks. Our approach was two pronged: we made Monte Carlo calculations to simulate the effect of the scattering continuum for our HPGe detector; and we also observed the source with a 30-mm² Si(Li) detector, which has higher resolution than our much larger HPGe detector.

Our calculations were performed with CYLTRAN, a Monte Carlo photon and electron transport code from the Integrated Tiger Series (ITS) [19], which is the same code we used in the precise calibration of our detector [15,16]. The input dimensions and properties of the HPGe detector were taken from direct measurements and were identical to those used in

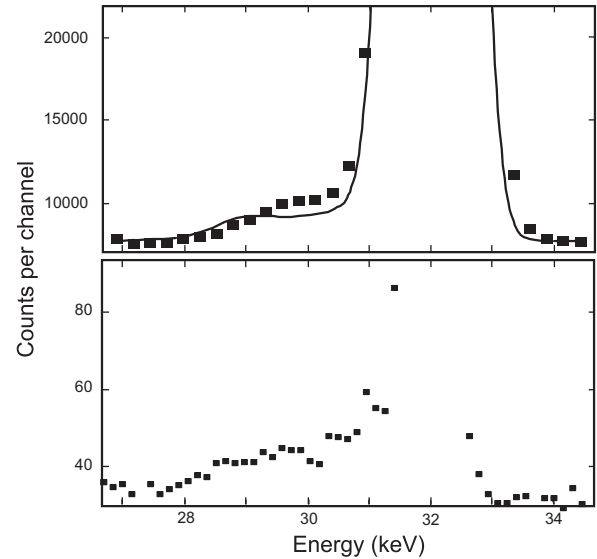


FIG. 5. The top panel shows an expanded region of the HPGe spectrum at the base of the barium K_{α} x-ray peak. The solid squares are the measured data from the ^{137}Cs source; the curve is the result of a Monte Carlo simulation. The bottom panel gives the same region of the ^{137}Cs spectrum as measured with a Si(Li) detector; the ordinate scale has been adjusted so that both panels display approximately the same fraction of the total K x-ray peak area.

the calibration. Since scattering was a particular concern for us in this experiment, we also modeled the source configuration and included a 1-m-diameter cylinder of air extending for 1 m in front of the detector face, completely surrounding the source, which was located 15 cm from the face. The Monte Carlo result, folded with a 1-keV (FWHM) Gaussian resolution function, is compared with the HPGe data in the top panel of Fig. 5. There it can be seen that the calculations give a reasonable representation of the continuum, although somewhat underestimating the effect overall. This is not surprising since the real world contained more objects—source holder, support tables, etc.—than could be modeled in the Monte Carlo calculation.

Since the primary Monte Carlo calculation was for a monoenergetic peak of zero width, we could easily determine from it that the continuum increased somewhat more as it approached the full-energy peak—i.e., where it would have been hidden in the 1-keV-resolution experimental data. To check this out, we measured our source in the identical geometry—15 cm from the detector face—with a higher resolution and much smaller Si(Li) detector. The result, in the bottom panel of Fig. 5, had limited statistics but unmistakably shows a slight rise in the continuum as the energy increases. (Since we did not have a reliable model of the Si(Li) detector, we did not attempt a separate Monte Carlo calculation for it.)

Now convinced that the Monte Carlo calculation was giving the correct energy dependence of the continuum, we analyzed the calculated spectrum that included the experimental resolution function to determine what fraction of the total continuum lay outside the peak under those conditions. By comparing our result with the known total content of the continuum, we could determine what fraction of the continuum lay hidden within

TABLE II. Evaluation of the ratio $\alpha_K(^{134}\text{Cs})/\alpha_K(^{137}\text{Ba})$.

Quantity	Value	Source
$(N_{K1}N_{\gamma2})/(N_{\gamma1}N_{K2})$	10.39(3)	Table I
Scattering correction (%)	-0.8(3)	Sec. IV E
Fully corrected ratio	10.31(4)	
ω_{K2}/ω_{K1}	1.007(2)	[12]
$\epsilon_{\gamma1}/\epsilon_{\gamma2}$	2.876(6)	[15]
$\epsilon_{K2}/\epsilon_{K1}$	1.0048(3)	Sec. II
$\alpha_{K1}(^{134}\text{Cs})/\alpha_{K2}(^{137}\text{Ba})$	30.01(15)	

the peak under experimental conditions. We then used that fraction to analyze the actual ^{137}Cs decay data. The resulting correction for the combined barium K_α and K_β x-ray peak areas was $-2.1(3)\%$.

Similar Monte Carlo calculations were performed for the $^{134}\text{Cs}^m$ source, including the additional Mylar and Kapton layers used in that case. This led to a rather higher scattering continuum with a slightly different shape. We determined the hidden fraction in the same way as we did for ^{137}Cs and analyzed the data accordingly. The correction to the cesium x-ray peak area was found to be $-2.8(4)\%$, slightly larger than for the barium x ray seen in the decay of ^{137}Cs . Since the same method was used to correct both these x-ray peaks, the principal uncertainty in the correction is systematic to both sources. As a result, we actually apply the correction to the x-ray ratio rather than to the individual peak areas, in which case it becomes $-0.8(3)\%$, the value used in Table II.

F. Lorentzian correction

As described in Sec. IV B, to be consistent with our previous efficiency-calibration procedures, we extracted our experimental peak areas using a special modification of the GF2 program that allows us to integrate the total counts above background within selected energy limits. To correct for possible missed counts outside those limits, the program adds an extrapolated Gaussian tail. We have already noted in a previous paper [9] that this extrapolated tail does not do full justice to x-ray peaks, whose shapes reflect the finite widths of the atomic levels responsible for them. As we did before, to correct for this effect we computed a simulated spectrum using realistic Voigt-function shapes for the x-ray peaks. Because we had analyzed the measured x-ray peaks as a group, in our simulation we generated the whole group with the tabulated relative x-ray intensities and then scaled them to the number of counts actually obtained in our experiment. The simulated spectrum was then analyzed with GF2 following exactly the same fitting procedure as was used for the real data. We could then compare the areas obtained by GF2 for the barium and cesium x-ray peaks with the actual peak areas used in the simulations. We found that 0.13% of the x-ray peak area was lost in each case, a small correction in itself but, being common to both peaks, completely negligible in the ratio. No correction for this effect was applied.

V. RESULTS AND DISCUSSION

The fully corrected ratio, $(N_{K1}N_{\gamma2})/(N_{\gamma1}N_{K2})$, appears in the third line of Table II. This is the value that now can be inserted into Eq. (2) in order to evaluate the final ratio of conversion coefficients, α_{K1}/α_{K2} . The other terms also required for that equation are listed in the subsequent three lines of the table together with the sources from which they were obtained. In all cases, the assigned uncertainties are conservative. In particular, for the fluorescence yields, individual values are quoted in Ref. [12] to 0.5% precision; however the values themselves are demonstrated to vary smoothly as a function of Z , so the percentage uncertainty on the ratio of two neighboring elements, whose ω_K values differ by only 0.7%, must surely be considerably smaller than the individual uncertainties. We conservatively assigned an uncertainty of 0.2% to the ratio. Our final result for the ICC ratio is given in the last line of the table.

In comparing this result to previous measurements, we refer to the recent survey [7] of world data on ICC values measured with an accuracy of better than 5%. The survey lists three previous measurements of α_K for the 127.5-keV transition in ^{134}Cs and ten for the 661.7-keV transition in ^{137}Ba . Unfortunately, in neither case are the measurements statistically consistent with one another: for the ^{134}Cs transition, the normalized chi-squared is 4.5; and for the one in ^{137}Ba it is 3.7. What the reviewers opted to do was to “adopt” recommended values based on their critical evaluation of the individual measurements rather than take rigorous statistical averages. Their adopted values were $\alpha_K(^{134}\text{Cs}) = 2.60(4)$ and $\alpha_K(^{137}\text{Ba}) = 0.0902(8)$, which leads to the ratio between them of 28.8(5). Our result is more than two standard deviations higher than this value and has an uncertainty less than one third as large. It is interesting to note, though, that if one were to take statistical averages of all the measurements listed in the survey [7], rather than use the adopted values, the ratio would have been 27.3(15), a significantly lower result with ten times the uncertainty of our measurement. Under the circumstances, we choose not to average our result with previous measurements.

Our measured ratio is compared with three different theoretical calculations in Table III. All three calculations are made within the Dirac-Fock framework, but one ignores the presence of the K -shell hole while the other two include it using different approximations: the frozen-orbital approximation, in which it

TABLE III. Theoretical values of α_K for the 127.5-keV $E3$ transition in ^{134}Cs and the 661.7-keV $M4$ transition in ^{137}Ba , together with their ratio, R , based on different theoretical models for dealing with the K -shell vacancy. Shown also are the corresponding percentage deviations, Δ , from the experimental value, $R(\text{expt}) = 30.01(15)$. For a description of the various models used to determine the theoretical ratios, see Ref. [9].

Model	$[\alpha_K]^{134}\text{Cs}$	$[\alpha_K]^{137}\text{Ba}$	R	Δ (%)
No hole	2.677	0.09068	29.52	1.6(5)
Hole, frozen orbitals	2.741	0.09148	29.96	0.2(5)
Hole, SCF of ion	2.730	0.09139	29.87	0.5(5)

is assumed that the atomic orbitals have no time to rearrange after the electron's removal; and the SCF approximation, in which the final-state continuum wave function is calculated in the self-consistent field (SCF) of the ion, assuming full relaxation of the ion orbitals. The percentage deviations given in the table indicate excellent agreement with both calculations that include the effects of the atomic vacancy, and disagreement by more than three standard deviations with the calculation that ignores the hole. Where the previous measurements showed some disagreement with all theoretical values and significant disagreement with those that included the hole, we now find just the opposite conclusion—and with significantly reduced error bars.

VI. CONCLUSIONS

We originally set out with this measurement to investigate one case—the 127.5-keV $E3$ transition in ^{134}Cs —in which previous experiments significantly disagreed with the most modern Dirac-Fock calculations whether or not the calculations took account of the conversion-electron hole. We wondered if there could be some undiscovered problems with the calculations unrelated to the atomic hole, which caused disagreement that was revealed only at the percent level of precision. Our result has definitively answered that question, at least for this transition, by demonstrating that experiment does in fact agree with the calculations.

As it has turned out, the high precision achieved in our measurement allows us to go a step farther and state that, once again, experiment shows a distinct preference for the calculation that makes the physically more reasonable assumption that the atomic vacancy persists until after the ejected electron has left the neighborhood of the atom. We have already shown [9,10] in the case of the 80.2-keV $M4$ transition in ^{193}Ir , where the hole and no-hole calculations of α_K differ by 10%, that the atomic hole must be taken into

account. Such a large difference in that case is the result of the low energy of the K -conversion electrons (~ 4 keV) from the 80.2-keV transition. However, this is the first time where it has been possible to draw the same conclusion for transitions with much higher energy K -conversion electrons—91.5 keV for ^{134}Cs and 624.2 keV for ^{137}Ba —where the difference is much smaller: viz. $\leq 2.3\%$ for ^{134}Cs and $\leq 0.9\%$ for ^{137}Ba . It is also the first test of the model among lighter nuclei. Of course, the statistical significance of the ^{193}Ir case—14 standard deviations—was much greater than the three-standard-deviation difference in this case. Nevertheless, the present result supports the contention that the Dirac-Fock approach, including provision for the atomic hole, provides the best available calculation, at least for α_K , over the full range of atomic numbers.

We also suggest, based on our result, that more of the old data included in the recent survey [7] may not stand up to modern experimental standards. The result upon which the surveyors principally based their adopted ^{134}Cs α_K value was published in 1961 [20]. Though meticulously executed and documented, the measurement used a NaI(Tl) detector and now long-outdated calibration standards. There may well be many other similarly anachronistic results in the survey, and it would make good sense to remeasure with modern equipment at least those other cases that show significant disagreement from what now appears to be a very effective theory.

ACKNOWLEDGMENTS

The work of the Texas A&M authors is supported by the U. S. Department of Energy under Grant No. DE-FG03-93ER40773 and by the Robert A. Welch Foundation under Grant No. A-1397. The work of M. T. is supported by the Russian Foundation for Basic Research under Grant No. 05-02-17340.

-
- [1] L. A. Sliv and I. M. Band, *Tables of Gamma-Ray Internal Conversion Coefficients*, Part I: K Shell (Acad. Sci. USSR, Moscow-Leningrad, 1956); Part II: L Shell (Acad. Sci. USSR, Moscow-Leningrad, 1958); see also in *Gamma Rays*, edited by L. A. Sliv (Acad. Sci. USSR, Moscow-Leningrad, 1961), p. 318 (in Russian); see also in *Alpha-, Beta-, and Gamma-Ray Spectroscopy*, edited by K. Siegbahn (North-Holland, Amsterdam 1958).
- [2] R. S. Hager and E. C. Seltzer, *Nucl. Data, Sect. A* **4**, 1 (1968).
- [3] F. Rösel, H. M. Fries, K. Alder, and H. C. Pauli, *At. Data Nucl. Data Tables* **21**, 91 (1978).
- [4] I. M. Band and M. B. Trzhaskovskaya, *Tables of Gamma Ray Internal Conversion Coefficients for K , L and M Shells*, $10 \leq Z \leq 104$, Leningrad Nuclear Physics Institute report, 1978 (in Russian).
- [5] I. M. Band, M. B. Trzhaskovskaya, C. W. Nestor, Jr., P. Tikkanen, and S. Raman, *At. Data Nucl. Data Tables* **81**, 1 (2002).
- [6] S. Raman, T. A. Walkiewicz, R. Gunnink, and B. Martin, *Phys. Rev. C* **7**, 2531 (1973).
- [7] S. Raman, C. W. Nestor, Jr., A. Ichihara, and M. B. Trzhaskovskaya, *Phys. Rev. C* **66**, 044312 (2002); see also the electronic addendum to this paper, the location of which is given in the paper's Ref. [32].
- [8] J. C. Hardy, N. Nica, V. E. Iacob, M. M. Trzhaskovskaya, and R. G. Helmer, *Appl. Radiat. Isot.* **64**, 1392 (2006).
- [9] N. Nica, J. C. Hardy, V. E. Iacob, S. Raman, C. W. Nestor Jr., and M. B. Trzhaskovskaya, *Phys. Rev. C* **70**, 054305 (2004).
- [10] N. Nica, J. C. Hardy, V. E. Iacob, J. R. Montague, and M. B. Trzhaskovskaya, *Phys. Rev. C* **71**, 054320 (2005).
- [11] J. H. Hubbell, P. N. Trehan, N. Singh, B. Chand, D. Mehta, M. L. Garg, R. R. Garg, S. Singh, and S. Puri, *J. Phys. Chem. Ref. Data* **23**, 339 (1994).
- [12] E. Schönfeld and H. Janssen, *Nucl. Instrum. Methods Phys. Res. A* **369**, 527 (1996).
- [13] Evaluated Nuclear Structure Data File maintained by the National Nuclear Data Center, Brookhaven National Laboratory: <http://www.nndc.bnl.gov>.
- [14] J. C. Hardy, V. E. Iacob, M. Sanchez-Vega, R. T. Effinger, P. Lipnik, V. E. Mayes, D. K. Willis, and R. G. Helmer, *Appl. Radiat. Isot.* **56**, 65 (2002).

- [15] R. G. Helmer, J. C. Hardy, V. E. Iacob, M. Sanchez-Vega, R. G. Neilson, and J. Nelson, Nucl. Instrum. Methods Phys. Res. A **511**, 360 (2003).
- [16] R. G. Helmer, N. Nica, J. C. Hardy, and V. E. Iacob, Appl. Radiat. Isot. **60**, 173 (2004).
- [17] D. Radford, <http://radware.phy.ornl.gov/main.html> (private communication).
- [18] C. T. Chantler, K. Olsen, R. A. Dragoset, J. Chang, A. R. Kishore, S. A. Kotochigova, and D. S. Zucker, X-Ray Form Factor, Attenuation and Scattering Tables, version 2.1 (2005), available online at <http://physics.nist.gov/ffast>.
- [19] J. A. Halbleib and T. A. Mehlhorn, Nucl. Sci. Eng. **92**, 338 (1986).
- [20] B. Keisch and E. A. C. Yates, J. Inorg. Nucl. Chem. **17**, 183 (1961).